Biosensors and Bioelectronics 258 (2024) 116315

Contents lists available at ScienceDirect

Biosensors and Bioelectronics

journal homepage: www.elsevier.com/locate/bios

Reduced graphene oxide electrodes meet lateral flow assays: A promising path to advanced point-of-care diagnostics

Enric Calucho [a,b], Ruslan Álvarez-Diduk [a,*], Andrew Piper [a], Marianna Rossetti [a], Tarja K. Nevanen [c], Arben Merkoçi [a,d,**]

[a] Nanobioelectronics & Biosensors Group, Institut Català de Nanociència i Nanotecnologia (ICN2), CSIC and the Barcelona Institute of Science and Technology (BIST), Campus UAB, Bellaterra, 08193, Barcelona, Spain
[b] Autonomous University of Barcelona (UAB), Bellaterra, Barcelona, Spain
[c] VTT Technical Research Centre of Finland Ltd., Tekniikantie 21, 02044, Espoo, Finland
[d] ICREA Institució Catalana de Recerca i Estudis Avançats, Passeig de Lluís Companys, 23, 08010, Barcelona, Spain

ARTICLE INFO

Keywords:
Electrochemistry
Lateral flow assays
Laser reduced graphene oxide
Scalable fabrication
Nanoflowers

ABSTRACT

Research in electrochemical detection in lateral flow assays (LFAs) has gained significant momentum in recent years. The primary impetus for this surge in interest is the pursuit of achieving lower limits of detection, especially given that LFAs are the most widely employed point-of-care biosensors. Conventionally, the strategy for merging electrochemistry and LFAs has centered on the superposition of screen-printed electrodes onto nitrocellulose substrates during LFA fabrication. Nevertheless, this approach poses substantial limitations regarding scalability. In response, we have developed a novel method for the complete integration of reduced graphene oxide (rGO) electrodes into LFA strips. We employed a CO_2 laser to concurrently reduce graphene oxide and pattern nitrocellulose, exposing its backing to create connection sites impervious to sample leakage. Subsequently, rGO and nitrocellulose were juxtaposed and introduced into a roll-to-roll system using a wax printer. The exerted pressure facilitated the transfer of rGO onto the nitrocellulose. We systematically evaluated several electrochemical strategies to harness the synergy between rGO and LFAs. While certain challenges persist, our rGO transfer technology presents compelling potential for setting a new standard in electrochemical LFA fabrication.

1. Introduction

In the realm of point-of-care (PoC) biosensors, lateral flow assays (LFAs) stand as a mature and universally recognized technology (Budd et al., 2023; Calucho et al., 2020; Parolo and Merkoçi, 2013). The past few decades have witnessed intensive efforts to enhance the sensitivity and quantification capabilities of LFAs, which are typically optical biosensors. However, LFA research remains vibrant and forward-looking, charting a course toward the next generation of these paper-based devices (Sena-Torralba et al., 2022). One of the current hot-topics in LFA research revolves around electrochemical detection.

Despite "primitive" instances of electrochemical detection in LFAs dating back to the turn of the century (Muhammad-Tahir and Alocilja, 2003), electrochemical LFAs are still in their nascent stages. It is therefore of no surprise that no commercially available LFAs currently operate using electrochemical detection strategies. The primary obstacle to their widespread adoption lies in the challenge of automating their fabrication. Recent reviews have compiled methods of integrating electrochemical transducers into LFAs (Cheng et al., 2022; Perju and Wongkaew, 2021). Almost without exception, the integration of electrochemical transducers into LFAs involved the simple overlay of an external electrode onto the nitrocellulose substrate of the LFA strip. Typically, these electrodes are screen-printed or consist of paper treated with inks. These electrodes may be placed atop the nitrocellulose, beneath it, or even on both sides in the case of a two-electrode system, with the nitrocellulose situated between them. The effectiveness of these assays hinges on the precise contact between the electrode and the LFA detection zone, as assay reproducibility is contingent upon it. The fact

* Corresponding author.
** Corresponding author. Nanobioelectronics & Biosensors Group, Institut Català de Nanociència i Nanotecnologia (ICN2), CSIC and the Barcelona Institute of Science and Technology (BIST), Campus UAB, Bellaterra, 08193, Barcelona, Spain.
E-mail addresses: ruslan.alvarez@icn2.cat (R. Álvarez-Diduk), arben.merkoci@icn2.cat (A. Merkoçi).

https://doi.org/10.1016/j.bios.2024.116315
Received 27 February 2024; Received in revised form 11 April 2024; Accepted 17 April 2024
Available online 24 April 2024

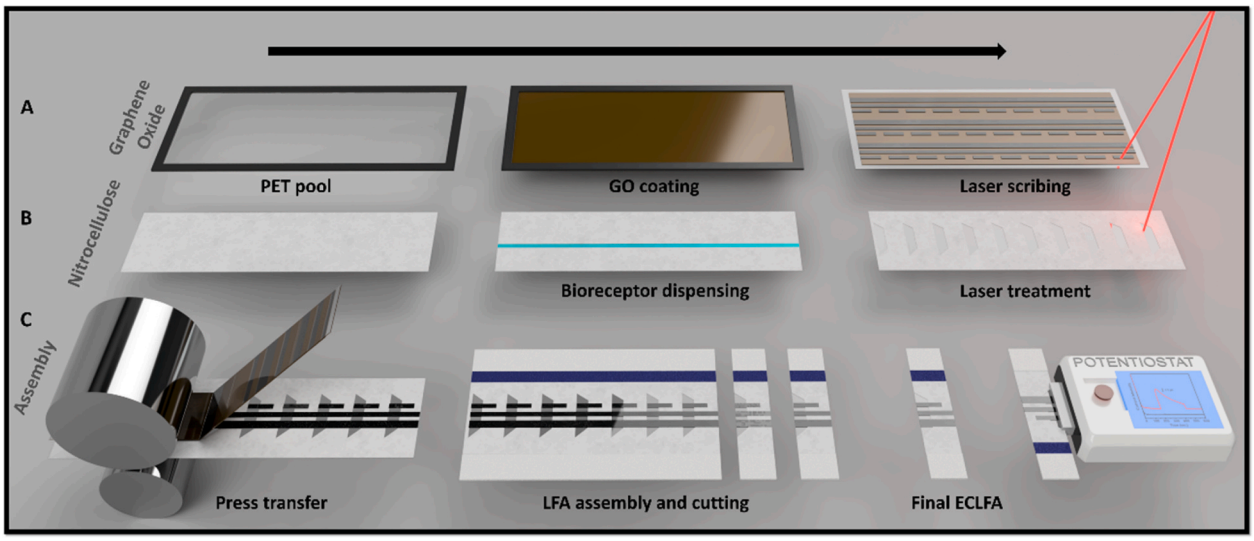

Fig. 1. Outline of the fabrication of electrochemical LFA strips. (A) GO is dried inside an ABS frame and reduced with a laser. (B) Concurrently, bioreceptors are dispensed on the nitrocellulose, once dry, the laser is applied to remove parts of the nitrocellulose membrane exposing the plastic below, which is going to become the support for the connection to the potentiostat. (C) Transfer of rGO to the nitrocellulose membrane, assembly of all the LFA pads, cutting into strips and connection to a potentiostat.

that the LFA strip and electrode are separate components hinders ease of fabrication and reproducibility. In some cases, measurement necessitates excising a segment of the strip for electrochemical analysis (Du et al., 2012). This practice persists to the present day (Deenin et al., 2023; Nandhakumar et al., 2023; Preechakasedkit et al., 2023), despite alternative methods that directly screen-print electrodes onto nitrocellulose (Ruiz-Vega et al., 2017), or metallize it using hydrofluoric acid and gold salts (Gonzalez-Macia et al., 2023); a process that could damage the nitrocellulose. Noteworthy is the application of microelectrodes in LFAs (Weiβ et al., 2022b), although it requires the use of clean room facilities for fabrication (Weiβ et al., 2022a).

Adopting a suitable electrode material and integration approach is therefore of paramount importance. Reduced graphene oxide (rGO) has features that make it desirable for electrochemical LFA integration, such as flexibility (Soni et al., 2018) and functional groups that can be exploited for biofunctionalization (Fu et al., 2017; Jang et al., 2022, 2023; Reiner-Rozman et al., 2016). Moreover, rGO is an affordable material, which is of relevance for LFAs, due to their PoC applicability. The main challenge is the transfer of rGO onto nitrocellulose. Previously, Baptista-Pires et al. reported a method in which vacuum-filtered GO was transferred from PVDF membranes to PET. However, their process involved water activation of GO, patterning with wax printing and chemical reduction. Moreover, the use of PVDF membranes does not make the process inherently scalable (Baptista-Pires et al., 2016). Such inconveniences can be avoided by laser-scribing of GO (El-Kady et al., 2012), which is a faster, cleaner and more flexible approach.

In this context, we present a straightforward, more scalable and cost-effective approach to seamlessly integrate electrodes into LFAs. Leveraging laser-based selective reduction and the transfer of rGO (Giacomelli et al., 2020), we can directly imprint rGO electrodes onto nitrocellulose without the need for solvents, rendering the process highly flexible. We also harness the capabilities of laser engraving to physically modify the strip, facilitating the connection to the potentiostat. Furthermore, nitrocellulose can be selectively removed to expose the plastic backing, onto which rGO can also be transferred. This approach significantly reduces the risk of sample leakage towards the connector, as the aqueous sample is naturally retained within the porous nitrocellulose. Consequently, the LFA strip and electrode become an inseparable entity. We have tested various sensing strategies to identify the most compatible approach for using rGO electrodes on nitrocellulose in electrochemical LFAs. Finally, we show a preliminary competitive LFA for cortisol, a stress biomarker (Hellhammer et al., 2009) that is also associated with Cushing's and Addison's syndromes. Patients with Cushing's syndrome exhibit elevated cortisol levels (Sakihara et al., 2010), while in contrast, hypocortisolism is characteristic of Addison's disease (Arlt and Allolio, 2003; Oelkers, 1996).

2. Materials and methods

2.1. Materials, reagents and equipment

Graphene oxide (GO) dispersions (1 wt%) were purchased from Graphenea (Spain). PET sheets were purchased from McDermid Autotype Ltd. (United Kingdom). Nitrocellulose membranes UniSart CN95 and CN150 with 100 μm polyester backing were purchased from Sartorius (Germany). Dielectric ink was purchased from Gwent Group (United Kingdom) Glass fiber and cellulose membrane (CFSP001700 and CFSP002000) were purchased from Merck Millipore (United States of America). Supporting adhesive backing cards were purchased from Kenosha (The Netherlands).

Bovine serum albumin (BSA), 10 mM phosphate buffer saline (PBS) tablets (137 mM NaCl, pH 7.4), sodium phosphate dibasic anhydrate, sodium phosphate monobasic monohydrate, sodium tetraborate decahydrate, boric acid, magnesium chloride, potassium ferricyanide, potassium ferrocyanide trihydrate diethanolamine (DEA), 1-naphthyl phosphate (1-NP), alkaline phosphatase (ALP), streptavidin-ALP conjugate, hydrocortisone (HC), anti-human IgG polyclonal antibody (I1886), human IgG (H-IgG), tetrachloroauric acid, iridium (III) chloride hydrate and sodium citrate were purchased from Merck Millipore (United States of America). All buffer solutions were prepared with Milli-Q water (Merck Millipore). Anti-cortisol (17) Fab fragments (regular and biotinylated) were provided by VTT (Finland) (Eronen et al., 2023). Cortisol-albumin conjugate was obtained from VTT (Finland) and purchased from Abyntek (Spain) as cortisol-BSA hapten.

The dispensing of bioreceptors onto nitrocellulose was performed with a BioSpot reagent dispenser prototype from BioFluidix (Germany). Nanoparticles centrifugation was performed with an Allegra 64R Centrifuge from Beckman-Coulter (United States of America), which was set up with a F2402H rotor (rMAX 82 mm). LFA strips were cut with a programmable strip cutter from Shanghai Kinbio Tech. Co. Ltd. (China). Acrylonitrile butadiene styrene (ABS) was printed with a BCN3D (Spain) 3D printer All operations involving laser treatment were performed with

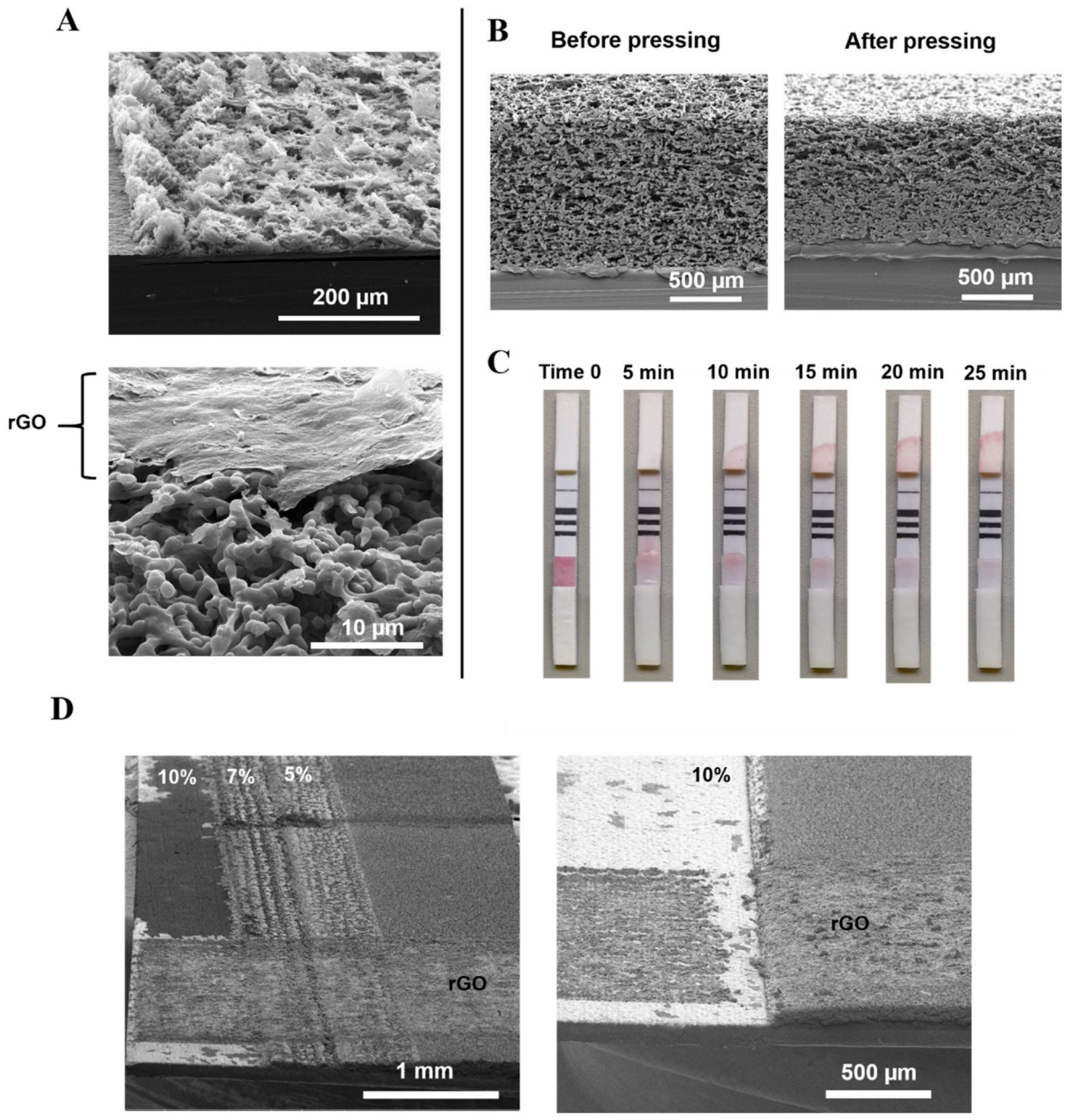

Fig. 2. (A) Top: SEM micrograph of rGO flakes after laser engraving the GO coating on PET. Bottom: SEM micrograph of rGO transferred onto nitrocellulose. (B) Morphological comparison of CN150 nitrocellulose before and after pressing with the die cutter. The pores after pressing are more compact and the effect on LFA fluidics is demonstrated in Figure S5. (C) Visual evaluation of the effect of transferring rGO with the roll-to-roll mechanism of the wax printer on AuNPs flowing through the LFA strip. At 25 min, all AuNPs have reached the sample pad and the nitrocellulose looks clean, thus indicating that the transfer method is compatible with standard fluidic behavior. Quadruplicates of this experiment are shown in Figure S6. (D) Left: rGO transferred onto nitrocellulose, which was previously treated with the laser at different powers (indicated within the micrographs) to create a staircase. There is a continuous, unbroken rGO layer. Right: rGO transferred onto untreated nitrocellulose. The abrupt change in height breaks the rGO track.

a Rayjet 50 laser engraver (CO_2 laser source, 10.6 µm wavelength, 0.04 mm spot size, 30 W power, 2" lens) from Trotec (Spain). Designs were made on Inkscape editor software. A ColorQube 8580 wax printer from Xerox (United States of America) was used to transfer rGO onto nitrocellulose. A DMM6500 Keithley Multimeter from Tektronix Company (United States of America) was used to measure resistance values. All electrochemical measurements, except where noted, were performed with a PalmSens4 potentiostat (The Netherlands) controlled with the 5.9 version of the PSTrace software. To analyze optically LFA strips after flow, pictures of the strips were taken with an OpticSlim 550+ from Plustek (Taiwan), which were analyzed with ImageJ. Scanning electron microscopy (SEM) was done with a Quanta 650 FEG from FEI (United States of America). Transmission electron microscopy (TEM), high-angle annular dark field (HAADF) scanning transmission electron microscopy (STEM) and energy dispersive X-ray spectroscopy (EDX) were performed with a Tecnai G^2 F20 from FEI (United States of America).

2.2. rGO electrode on LFA design and fabrication

The workflow followed to fabricate electrochemical LFA strips is outlined in Fig. 1 (Figure S1 shows pictures of the actual process and its materials), consisting of two parallel procedures. On one hand there is the dispensing of bioreceptor followed by the removal of nitrocellulose with the laser, and on the other hand the drying of GO and subsequent reduction, also with the laser. Both pathways converge in the transference of rGO onto nitrocellulose. In this section, the steps that are

relevant to the work's novelty will be detailed. Parts of the protocol related to the fabrication of the LFA strips (nanoparticle synthesis, conjugation and pads preparation) are included in the Supporting Information.

2.2.1. Conditioning of the nitrocellulose

A Rayjet 50 CO_2 laser was used to remove nitrocellulose from the membrane, leaving trapezoidal windows periodically. This was done to allow connection of the rGO electrodes to a potentiostat in an area where the sample solution could not wick and short the connection. Laser power and speed were set to 10 and 100% respectively (corresponding to 2.39 kW/mm^2 and 1.5 m/s), conditions under which nitrocellulose is completely removed. Pulses per inch (PPI) were fixed at 500 PPI. The window shape was selected to allow a smooth flow of the samples from the sample pad. Since the total removal of nitrocellulose creates a "step" that is too high for the transferred rGO to pass over without breaking (Figure S2), two intermediate steps were created by partially removing nitrocellulose. For each partial removal, the laser power was set to 7 and 5% (1.67 and 1.19 kW/mm^2). Additionally, two small marks were made in order to aid the alignment of the nitrocellulose and the rGO (Figure S3).

At the end of treatment, the electrochemical LFA strips are 7 mm-wide and feature a trapezoidal area on their left flank in which nitrocellulose has been totally or partially removed (Fig. 2B). The exact size specifications of the laser modifications are provided in Figure S4A.

2.3. Preparation and transference of rGO onto nitrocellulose

A 9 cm × 5 cm piece of PET, which can fit up to 30 electrodes, was immobilized on a ceramic surface with double-sided tape. An ABS 3D-printed rectangular frame with inner dimensions of 8 cm × 4 cm and external dimensions of 10 cm × 6 cm was placed on top of the PET piece, thus forming a "pool" with a depth of 2 mm. In the volume comprised within the frame, 6 mL of GO was drop-cast and left to dry overnight at 37 °C. The dry GO was selectively reduced with the laser to pattern three long lines corresponding to counter, reference and working electrode (Fig. 1). Exact dimensions of each electrode in the final strips are specified in Figure S4B.

In order to transfer the rGO onto the nitrocellulose membranes (which had already the test line (TL) dispensed; Supporting Information), the roll-to-roll mechanism of a wax printer was used to apply the necessary pressure. The nitrocellulose and the PET piece with rGO were fixed facing each other on a piece of paper with tape, prior to introducing the whole ensemble into the printer. Other transfer methods have been attempted, namely a dye cutter and a laminator, but did not work as well as the wax printer (see Results and Discussion section).

2.4. Assembly of the LFA strips

The nitrocellulose membrane with the transferred rGO and the conjugate, sample and absorbent pads were assembled on a laminated card, following previously established protocols (Parolo et al., 2020). The preparation of each pad is explained in Supporting Information.

2.5. Electrochemical characterization of the rGO electrodes

The rGO transferred onto nitrocellulose was characterized by performing cyclic voltammetry (CV) in a solution of 10 μL 5 mM of $[Fe(CN)_6]^{3-/4-}$ in PBS 10 mM pH 7.4 dropped near the 3 electrode working area. CV was performed for 5 scans between −0.4 V and +0.4 V vs the on board pseudo reference rGO at varying scan rates always with a 10 mV potential step.

In order to assess the compatibility of the electrodes with an enzymatic approach, we mixed ALP and its substrate 1-NP, whose product is the electroactive 1-naphthol (1-N). The mix was prepared in 0.1 M DEA buffer (1 mM $MgCl_2$, pH 9.8). 1-NP concentration was fixed at 5 mM, while ALP was tested at three dilution factors from its stock concentration (x20, x200, x2000). Differential pulse voltammetry (DPV) was recorded on the electrodes every 5 min after the mix was prepared. For each measurement, 10 μL of the mix were loaded onto the electrodes. The DPV parameters were set as follows: initial potential, −0.4 V; end potential, +0.9 V; potential step, 10 mV; potential pulse, 175 mV; pulse, 300 ms; scan rate, 10 mV/s.

Au–IrO_2 nanoflowers (NFs) were also used to assess alternative electrochemical detection strategies in LFA. Their synthesis is detailed in the Supporting Information. For the direct detection of Au–IrO_2 NFs by oxidation and subsequent reduction of gold, 15 μL of nanoparticles dispersion were mixed with 15 μL of HCl (0.2 M) and flown through the nitrocellulose. After 2 min applying +1.25 V, DPV was performed with an Autolab PGSTAT 302 (Metrohm, Switzerland) with the following settings: step, 1 mV; modulation amplitude, 50 mV; modulation time, 50 ms; interval time, 0.1 s. Similarly, Au–IrO_2 NFs were also loaded onto the electrodes without HCl and then CVs were performed from −0.2 V to +1.0 V with a scan rate of 50 mV/s.

2.6. Electrochemical measurements in LFA

Cortisol (HC for hydrocortisone in medical terminology) samples in PBS 10 mM (137 mM NaCl, pH 7.4) were used as the proof-of-concept target analyte. For final measurements performed in fully assembled LFA strips with integrated rGO electrodes, 150 μL of sample was loaded on the sample pad. After 30 min of flow, 5 μL of 1-NP (5 mM), was carefully added next to the TL onto the nitrocellulose (detection pad of the strip), taking caution to not overload it. After 5 min, DPV was performed using the setting described above.

3. Results and Discussion

3.1. Transfer of rGO electrodes and its effects on LFA fluidics

We investigated the morphology of the rGO electrodes after they were transferred onto nitrocellulose by SEM. Fig. 2A illustrates the results, revealing that the laser-based reduction of GO led to the formation of highly exfoliated structures. These structures are readily detachable when pressure is applied to another surface (Giacomelli et al., 2020; Scroccarello et al., 2023; Zhao et al., 2023).

The successful transfer of rGO onto nitrocellulose necessitates careful consideration of the method used to apply pressure. This is crucial to prevent any disruption in the fluidics of the nitrocellulose substrate. Excessive pressure could flatten the pores of the nitrocellulose, rendering it unsuitable for use in LFAs, even if rGO is perfectly transferred. Conversely, applying insufficient pressure may not achieve effective rGO transfer. Striking a pressure "sweet-spot" for optimal transference and fluidics is, therefore, imperative. This consideration was not as critical in previous works where tons of pressure were applied to make the transfer, as the receiving substrate did not serve an additional fluidic function (Giacomelli et al., 2020; Scroccarello et al., 2023; Zhao et al., 2023).

We explored several methods to address this challenge, including a die cutting machine for crafting, a laminator, and the roll-to-roll mechanism of a wax printer. When employing a die cutter, rGO is transferred successfully. However, the pressure applied is excessive, leading to LFA strips that do not flow properly (see Figure S5) due to compacting of the nitrocellulose, as the SEM micrographs in Fig. 2B illustrate. On the other hand, the laminator fails to apply sufficient pressure to facilitate rGO transfer. Finally, the roll-to-roll mechanism proves to be the optimal choice, providing the right amount of pressure for effective rGO transfer while preserving the fluidic properties of the nitrocellulose substrate. Movie 1 shows the simplicity of the method and a successful transfer of rGO onto nitrocellulose. Moreover, as illustrated in Fig. 2C and Figure S6, the resulting LFA strips featuring transferred rGO lines retain their wicking properties. After the addition of PBS to

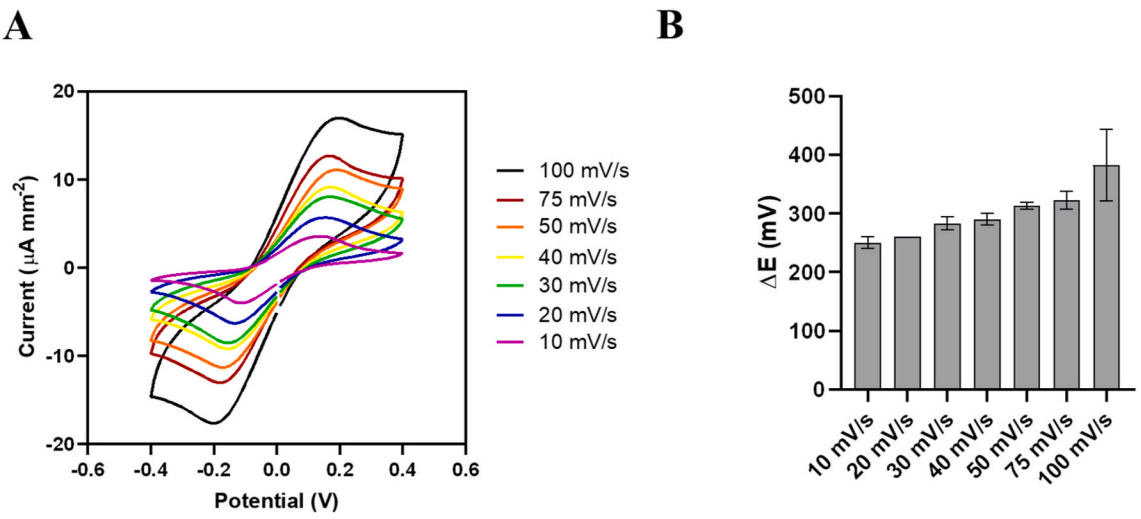

Fig. 3. Electrochemical characterization of the rGO electrodes on nitrocellulose. Experiments were performed in triplicate. (A) Cyclic voltammograms in 5 mM $[Fe(CN)_6]^{3-/4-}$ (PBS 10 mM, pH 7.4) at different scan rates. (B) Oxidation and reduction peak separation at each scan rate.

release the gold nanoparticles (AuNPs) from the conjugate pad, the majority of the AuNPs reach the sample pad within the standard LFA operating time of 25 min (Movie 2). Additionally, the strips maintain their cleanliness, further indicating that the fluidics of the nitrocellulose are unimpeded.

Supplementary video related to this article can be found at https://doi.org/10.1016/j.bios.2024.116315

3.2. Reproducibility of the rGO transference

Following the selection of the transfer method, the laser-induced reduction of GO and its subsequent transference had to be optimized. To accomplish this, 6 cm long lines, each 1 mm in width, were engraved on the dry GO and then transferred to a piece of nitrocellulose using the roll-to-roll method. This process was conducted at a fixed laser speed of 100% (1.5 m/s) while varying the laser power from 4% (0.95 kW/mm^2) to 13% (3.10 kW/mm^2) in 1% (0.24 kW/mm^2) increments. Pulses per inch (PPI) were fixed at 500 PPI. After the rGO was successfully transferred, the resistance at each 1 cm segment was measured using a multimeter. As illustrated in Figure S7, insufficient laser power fails to fully reduce the GO, while excessive power leads to the removal of rGO from the PET substrate. Moreover, increasing the power results in lower resistance values for the rGO, rendering its values more consistent along the longitudinal axis of the nitrocellulose piece until a threshold power level is reached, after which the values become more variable again, due to the potential removal of rGO from PET. The optimal power level was found to be 11% (2.63 kW/mm^2), resulting in a mean resistance of 1.54 kΩ (±0.19).

3.3. Design considerations for electrochemical LFA strips

In the process of developing electrochemical LFAs, the connection to the potentiostat is often given little consideration because, in most cases, an electrode and an LFA strip are simply stacked together, with the connector tracks of the electrode protruding. However, following the roll-to-roll method for rGO transfer, the entire electrode is in direct contact with the nitrocellulose. Consequently, any sample added to an LFA strip made from this material may potentially seep into the potentiostat's connectors through capillarity. To address this issue, a barrier must be implemented to prevent such leakage.

Initial approaches involved manually drawing dielectric ink barriers with a micropipette tip. However, this method was highly time-consuming as each LFA strip/electrode had to be prepared individually. This process evolved into a more scalable version using a screen-printing mask (see Figure S8A). However, it did not consistently prevent leakage. An alternative approach, printing wax and then melting it with heat, was considered. However, this method had a negative impact on the rGO transference (Figure S8B). It was during this exploration that we discovered the most effective solution: eliminating the need for a barrier altogether. This was achieved by selectively removing the nitrocellulose with a laser, creating windows that expose its polyester backing. The specific dimensions of these windows on each LFA strip can be found in Figure S4A. Subsequently, rGO can be transferred to both the nitrocellulose and the polyester backing without altering the transfer method. To ensure the continuity of the rGO tracks, partial removal of nitrocellulose was also necessary, which was achieved by creating nitrocellulose steps with lower laser powers. Fig. 2D illustrates the effect of transferring rGO with (left) and without (right) these steps. This approach is highly compatible with the rest of the fabrication process and inherently scalable.

3.4. Electrochemical characterization

Prior to their integration into LFA strips, we conducted a thorough assessment of the rGO electrodes on nitrocellulose to determine their suitability for electrochemical sensing. Given that LFAs involve the flow of samples within the nitrocellulose, it is crucial that the rGO electrodes remain responsive in this configuration, meaning that they function effectively when positioned atop the nitrocellulose.

To assess this, we carefully made 10 μL of 5 mM $[Fe(CN)_6]^{3-/4-}$ in PBS (10 mM) flow into the nitrocellulose, ensuring that all of it was adequately wet without any liquid on the top of the rGO electrodes themselves. All the solution was at the rGO/nitrocellulose interface, not the rGO/air interface. We then performed CV at a range of scan rates. The system containing $[Fe(CN)_6]^{3-/4-}$ exhibited quasi-reversible behavior, as evidenced by the substantial separation between the reduction and oxidation peaks, which exceeded 59 mV (Fig. 3) and, more specifically, surpassed 250 mV (Tanimoto and Ichimura, 2013).

To delve deeper into the assessment of the rGO electrodes on nitrocellulose, we applied the Randles-Sevick equation to calculate the electroactive area, which was determined to be 0.96 ± 0.13 mm^2. This value suggests a slight reduction from the geometrical area (1.25 mm^2) for the working electrode, likely attributed to some surface area being in contact with the nitrocellulose fibers rather than being exposed in the pores. Nevertheless, even in this scenario, we observed a diffuse-controlled electron transfer, as indicated by the current linearly

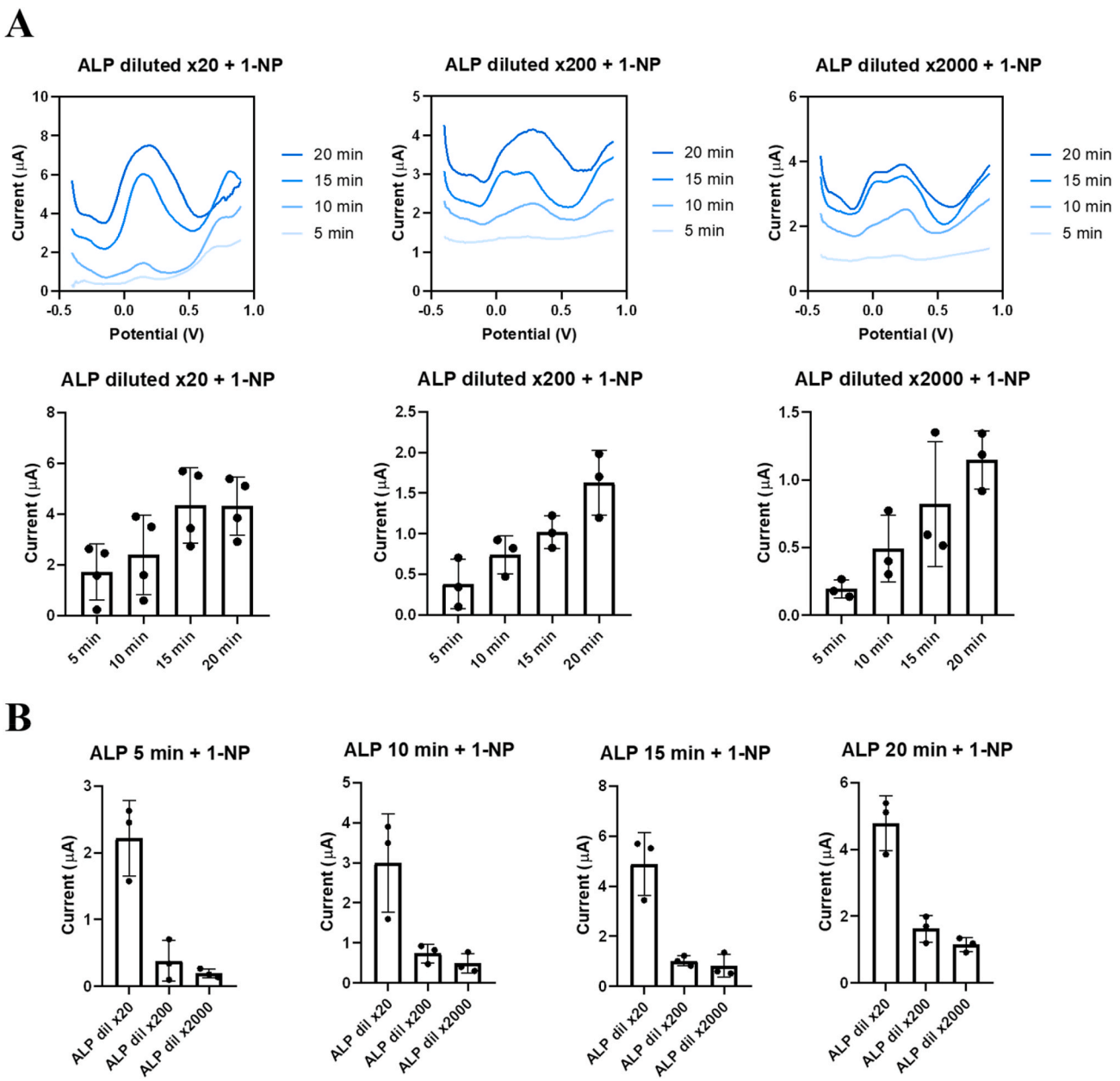

Fig. 4. Characterization of rGO electrodes on nitrocellulose with ALP-based enzymatic approach. Dilutions of the ALP stock solution (x20, ×200 and x2000) were studied to assess the potential of ALP to provide an analytical signal in electrochemical LFA. (A) Differential pulse voltammograms after mixing ALP with a fix concentration of 1-NP (5 mM). Column graphs represent the peak height at every 5 min after mixing. Experiments were performed in triplicate. (B) Peak height of the same differential pulse voltammograms as a function of ALP dilution factor.

increasing with the square root of the scan rate (Elgrishi et al., 2018). The Randles-Sevcik equation is based on the semi-infinite linear diffusion of redox molecules to the electrode surface. Since these electrodes are on the surface of a nitrocellulose membrane where the solution has other mass transport properties, namely the flow through the membrane, we would not expect complete agreement with the Randles-Sevcik equation. However, getting a value within the same order of magnitude does convince us that we have a decent proportion of the working electrode in good contact with the solution at the nitrocellulose/electrode interface. A full analysis of the flow within the membrane and its effect on the electrochemical response is the topic of ongoing research and beyond the scope of this paper. It is also encouraging that we get decent electrochemical responses in that the pseudo-reference and counter electrodes are transferred and working, also that the connections are satisfactory.

Additionally, we extended our study to investigate the relationship between the rGO electrodes and a diffusing redox probe within an assembled LFA strip. In these strips, equipped with sample and absorbent pads, we loaded PBS followed by 5 mM $[Fe(CN)_6]^{3-/4-}$ after 1 min. We conducted CV at a scan rate of 40 mV/s until the strips dried out. Figure S9 presents the evolution of the oxidation peak over time. In the initial 10 min, we observed an increase in the oxidation peak height, attributed to the arrival of the solution front under the rGO electrode area. In this front, there is a greater concentration of $[Fe(CN)_6]^{3-/4-}$, due to increased evaporation and flow. Subsequently, over the next 5 min, the oxidation peak height decreased, remaining stable for the following 50 min because the $[Fe(CN)_6]^{3-/4-}$ concentration remains constant and the only fluid dynamics are coming from the constant wicking through the absorbent pad and the evaporation. After this period, the oxidation peak gradually increased to more than double its previous values. We

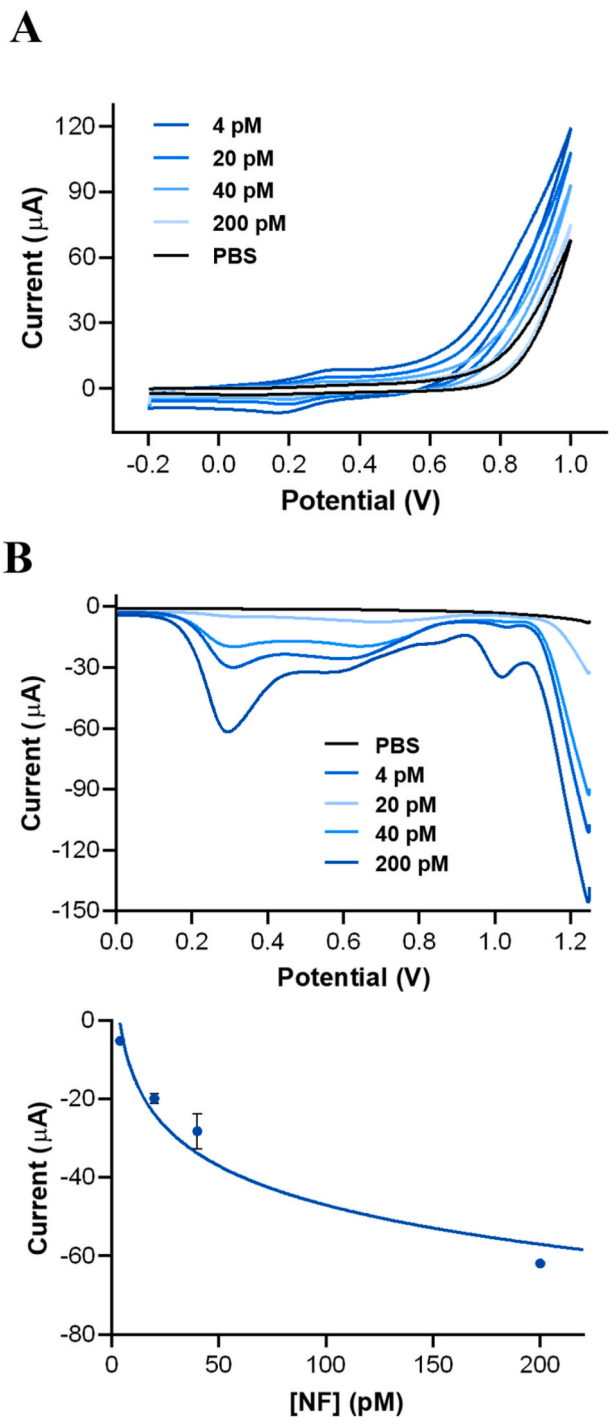

Fig. 5. (A) Cyclic voltammograms with increasing concentrations of Au–IrO_2 NFs, catalyzing the water oxidation reaction. (B) Top: Differential pulse voltammograms for the direct detection of gold, by oxidizing for 2 min after the addition of HCl (0.2 M) and applying +1.25 V. Bottom: Reduction peak height at +0.3 V from the previous voltammograms.

hypothesize this is due to a gradual drying of the strips, which leads to a reconcentration of $[Fe(CN)_6]^{3-/4-}$. Finally, at the 100-min mark, as the oxidation peak height begins to stabilize, it experiences a sharp decline due to the complete drying of the strips.

In the enzymatic approach, we selected ALP as the enzyme. This choice was based on the fact that one of its commonly used substrates, 1-NP, is not electroactive within the tested range, while its product, 1-N, can be detected at potentials ranging from 0 V to +0.3 V (vs Ag/AgCl) through DPV (Kudr et al., 2020; Ricci et al., 2012). In the case of the rGO electrodes on nitrocellulose, the presence of ALP enabled the detection of 1-N as early as 5 min after mixing. The oxidation peak height increased with increasing mixing time, which is expected from an enzymatic reaction (Fig. 4A). Furthermore, at each time point, samples with a lower ALP concentration (higher dilution factor) generated lower oxidation peaks due to the resulting lower 1-N concentration (Fig. 4B). These results support the potential applicability of enzymatic approaches in electrochemical LFAs.

Notably, Au–IrO_2 NFs, which have only recently been used in LFAs as optical labels (Rivas et al., 2023), are known to possess interesting electrochemical (Zhao and Fan, 2012) and light harvesting capabilities (de Freitas et al., 2020). This combination suggests the possibility of dual electrochemical and optical readouts. In terms of optical detection, Au–IrO_2 NFs offer significant promise, as they have been reported to yield lower limits of detection (e.g., 8.5-fold for H-IgG) (Rivas et al., 2023). From an electrochemical perspective, Au–IrO_2 NFs can be harnessed for their individual components. Gold can be oxidized to Au^{3+} cations under acidic conditions and reduced through DPV (De La Escosura-Muñiz et al., 2011). Meanwhile, iridium oxide is known to serve as a catalyst for the water oxidation reaction (WOR) at sufficiently oxidizing potentials (Rivas et al., 2014).

The synthesized Au–IrO_2 NFs were characterized in TEM to confirm their correct synthesis by observing their characteristic flower-like shape (Figure S10A). Additionally, the presence of Au and Ir was confirmed with EDX in HAADF-STEM mode (Figure S10B). We loaded Au–IrO_2 NFs onto the rGO electrodes transferred onto nitrocellulose, and the resulting signal was examined at different concentrations. Fig. 5 summarizes the results, exploiting the catalytic properties of iridium oxide by inducing oxidative potentials through CV (A) and directly detecting gold content through DPV (B). In light of the observed behavior, DPV was selected as a more sensitive and reproducible technique for experimenting in full LFA format, despite the need of the additional step of adding HCl to reduce the pH.

3.5. Electrochemical measurements in LFA

The results so far demonstrate that rGO electrodes on nitrocellulose are able to respond to different electroactive labels (i.e. $[Fe(CN)_6]^{3-/4-}$, 1-N via ALP-mediated catalysis and Au–IrO_2 NFs), including during flow with $[Fe(CN)_6]^{3-/4-}$. In order to assess the potential of rGO electrodes to be applied in LFA, we opted to use Au–IrO_2 NFs functionalized with ALP. This approach was selected since it would yield a colorimetric readout from the NFs, and an electrochemical readout from the enzyme. We hypothesized that the enzymatic approach would allow the diffusion of the electroactive product within the LFA membrane, which would be beneficial for sensing as we are not just measuring the surface confined transductors. Cortisol detection is achieved in a competitive manner; in which the cortisol in the sample competes for the binding by the NF conjugates against a cortisol-BSA hapten deposited as a TL. Therefore, the blank samples generate a greater signal since a higher quantity of Au–IrO_2 NF conjugates could potentially bind to the TL, see Fig. 6A. As the concentration of cortisol in the sample increases, the NF conjugates bind to it and then flow across the TL, unable to bind the cortisol-BSA since their cortisol binding fragments are already bound to the cortisol from the sample. First, we explored the conjugation of Au–IrO_2 NFs with anti-cortisol (17) Fab and ALP at two different ALP concentrations (4 and 0.4 μg/mL). The conjugation procedure and TL preparation are detailed in the Supporting Information. LFA strips were prepared with conjugate pads under both conditions and were tested in triplicate with PBS, followed by the addition of 1-NP in the detection pad near the TL and working electrode zone after sample flow. The results obtained are presented in Figure S11, demonstrating that the strips with ALP at 4 μg/mL during the conjugation step exhibited a stronger response compared to those with ALP at 0.4 μg/mL, as anticipated.

An alternative conjugation in which the anti-cortisol Fab was

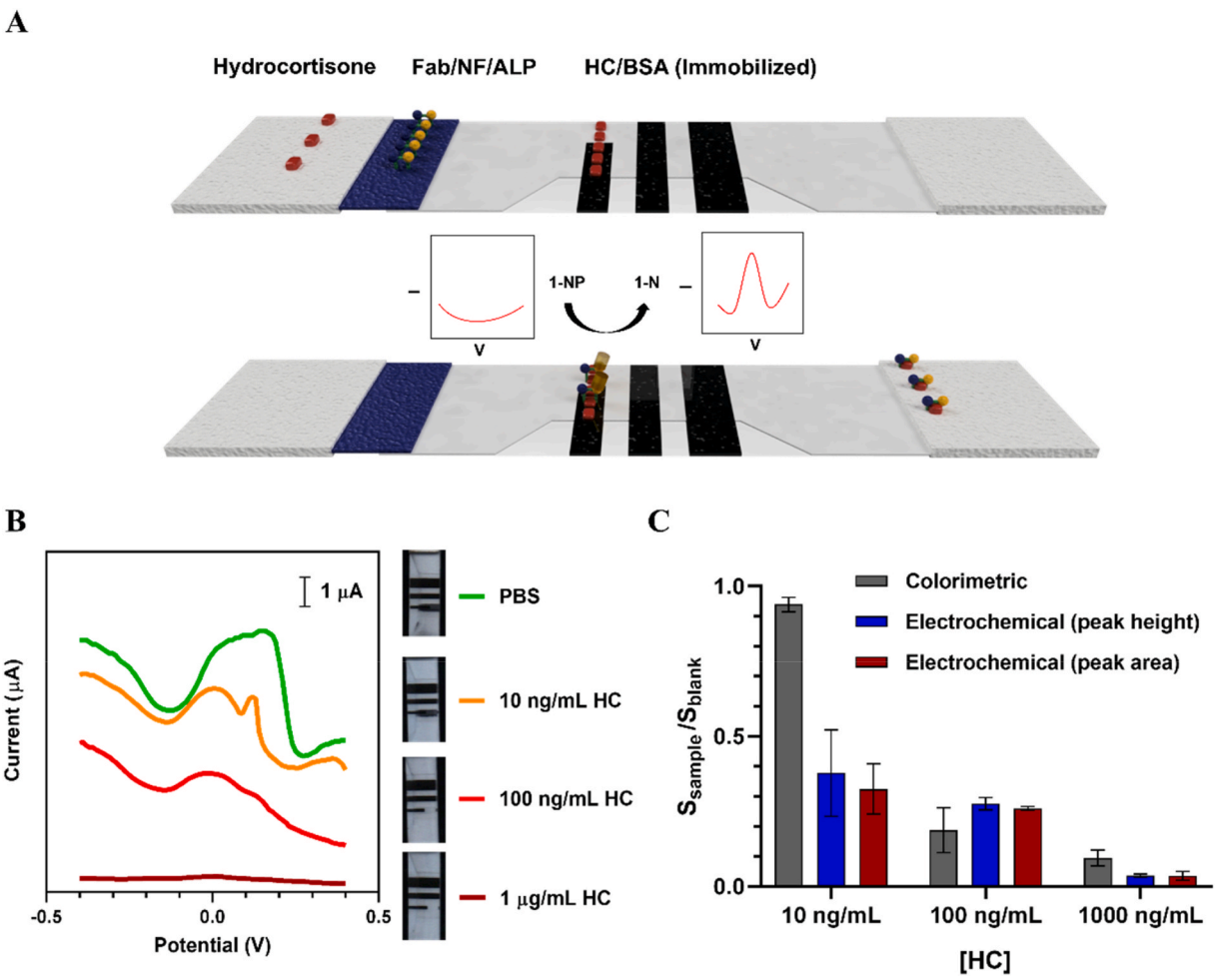

Fig. 6. Comparative results of optical and electrochemical measurements with electrochemical LFA strips. (A) Schematic representation of the enzymatic approach with ALP. After loading a sample containing HC, the Au–IrO_2 NFs conjugated to ALP and anti-cortisol (17) Fab are accumulated at the TL. 5 mM 1-NP, which is not electroactive, is then loaded onto the nitrocellulose near the TL and working electrode (5 μL), and after 5 min, 1-N, the product of the enzymatic reaction, can be detected with DPV. (B) Qualitative comparison of DPV peaks with their naked eye colorimetric counterparts. Colorimetric signal is provided by Au–IrO_2 NFs (dark grey colored band next to the working electrode), which are conjugated to ALP and anti-cortisol (17) Fab. (C) Normalized values of colorimetric (n = 6) and electrochemical (n = 2) readouts represented as signal remnant respect the blank, considering the blank sample elicits the maximum signal response. The error bars are the propagated standard deviations from the blanks and samples since the values shown are normalized.

biotinylated and attached to ALP-streptavidin, before being adsorbed onto the NFs was also investigated. In this approach the anti-cortisol (17) Fab concentration was maintained to be comparable with the previous data, while the ALP-streptavidin stock solution was diluted at a 1:2000 ratio. This modified conjugation process appeared to enhance the yield, as suggested by the subsequent LFA results (Figure S12). After the addition of 1-NP, the strips tested with PBS generated a greater signal compared to those tested with HC, as would be expected in a competitive assay format. This conjugation method was selected for further measurements.

A comparative analysis of the optical and electrochemical readouts from these LFAs was performed by measuring different concentrations of HC (Fig. 6). A schematic of how the LFA operates is given in Fig. 6A. The electrochemical response at different HC concentrations, along with pictures of the strips showing the rGO electrodes and the corresponding TL for the same concentrations is provided in Fig. 6B. Full optical results are provided in Figure S13. At 10 ng/m HC the optical signal is the same within error as the blank response, while for electrochemical readouts the signal decreases to 40% of the blank's signal, suggesting that the electrochemical response can achieve lower limit of detection. For 100 ng/mL HC samples, the optical readout takes a huge leap down to roughly 20% of the blank's signal. However, the decrease in electrochemical readout is more gradual. For 1000 ng/mL HC samples, the electrochemical response decreases to become almost non-existent, while the optical response is still 10% of the response from the blank sample. These results show that, for this particular dual approach, optical and electrochemical readouts work over different dynamic ranges. Roughly from 10 to 100 ng/mL in the optical readout (see Figure S13 for specific values), and shifting to lower values for the electrochemical readout. This is an important finding as it hints at the possibility to expand the overall dynamic range of point-of-care sensors.

It should be noted that in the 10 ng/mL HC concentrations, we observe more variability in the electrochemical signals. Future work will focus on improving the reproducibility, particularly at low sample concentrations.

Unsurprisingly, each readout will have its own optimal conditions, such as: nanoparticle conjugation method, bioreceptor concentration, dynamic range, electrode dimensions. Nonetheless, due to the interdependency of the variables at play, it is unlikely that the optimal conditions for one transduction method will be optimal for the other, and so a balance between must be struck. This requires optimization of both readout methods in tandem, which complicates sensor development.

4. Conclusions

In this study, we present an innovative and scalable method for the fabrication of LFA strips with intimately integrated rGO electrodes. We capitalize on the selective laser engraving of GO and its subsequent transfer onto nitrocellulose under dry conditions. Laser engraving is also employed to partially remove nitrocellulose, allowing rGO to be transferred onto the polyester backing and facilitating a leak-free connection site. The optimal rGO transfer is achieved by applying pressure with the roll-to-roll mechanism of a wax printer. While the entire process may be considered physically intensive, it is also highly automated and elegant, demonstrating that classical LFA capabilities of fluidics and biorecognition are preserved.

We have explored several electrochemical approaches to gain a deeper understanding of how rGO electrodes function when transferred onto nitrocellulose, a porous matrix. The use of nanoparticles to directly elicit electrochemical signals was not the most suitable, as we hypothesize that they remain too distant from the electrode surface, impeding electron transfer (see Figure S14). However, this characteristic is inherent to the traditional operation of LFAs, where nanoparticles accumulate throughout the strip within a defined space (the TL). Therefore, our electrodes, in their current form, are better suited for smaller freely diffusing electroactive molecules, prompting us to work with an enzymatic approach, in which the reaction product remains free in solution within the nitrocellulose fibers, in contrast to Au–IrO_2 NFs.

As far as this work goes, the simultaneous optical and electrochemical readout has been demonstrated in LFA. Although improvements should be made in terms of sensitivity, we want to emphasize that there is still a lot to explore in terms of fabrication processes, and scalable methods are indispensable if there is real intent to launch electrochemical LFAs to the market.

Despite the promising data, we have encountered new challenges. The main drawback of the enzymatic approach lies in the additional steps it requires, introducing second-order variables, such as determining the optimal position within the strip for substrate addition and whether the electrode should be rewetted before measurement, among others. Moreover, however automatized the fabrication of strips has been made, it still requires manual adjustments to properly align the rGO and nitrocellulose in the transfer step. While the roll-to-roll method has proven to be an effective solution to consistently apply the same pressure, it is fair to acknowledge that it is not a tailor-made solution to the problem, merely showing that the process is feasible since an optimum pressure does exist. Consequently, we hypothesize that these intrinsic characteristics of the fabrication method, coupled with the generally accepted sensitivity of electrochemical measurements, contribute to the risk of reduced sensitivity of the signal obtained after sample testing. Nevertheless, this does not diminish the potential for establishing a new paradigm for electrochemical LFA fabrication using rGO transfer technology, properly adapted to meet the specific requirements of nitrocellulose.

The possibilities in this field are vast, and the complexities of each approach make it highly exciting, both in terms of fabrication and the available electrochemical techniques. Future work to address the challenges of electrochemical LFAs with rGO electrodes will focus on the direct biofunctionalization of electrodes with bioreceptors before transference. This approach aims to facilitate electron transfer on the electrode surface and may involve nanostructured rGO electrodes with embedded AuNPs (Scroccarello et al., 2023). Although this implies additional treatment of the rGO, potentially sacrificing some ease of fabrication, it is expected to lead to performance improvements.

Notes

The authors declare no competing financial interests.

CRediT authorship contribution statement

Enric Calucho: Writing – original draft, Methodology, Investigation, Formal analysis, Data curation. **Ruslan Álvarez-Diduk:** Writing – review & editing, Visualization, Supervision, Methodology, Investigation, Conceptualization. **Andrew Piper:** Writing – review & editing, Methodology. **Marianna Rossetti:** Writing – review & editing, Formal analysis. **Tarja K. Nevanen:** Writing – review & editing, Investigation. **Arben Merkoçi:** Writing – review & editing, Supervision, Resources, Funding acquisition.

Declaration of competing interest

The authors declare that they have no known competing financial interests or personal relationships that could have appeared to influence the work reported in this paper.

Data availability

No data was used for the research described in the article.

Acknowledgements

This work has received funding from the European Union's Horizon 2020 research and innovation programme under the Graphene Flagship grant agreement no. 881603. The support received is also acknowledged by R. Alvarez. Views and opinions expressed are however those of the authors only and do not necessarily reflect those of the European Union. The European Union cannot be held responsible for them. This project has received funding from the European Union's Horizon Europe – the Framework Programme for Research and Innovation (2021–2027) under grant agreement No 101120706. Views and opinions expressed are however those of the author(s) only and do not necessarily reflect those of the European Union. Neither the European Union nor the granting authority can be held responsible for them. The ICN2 is funded by the CERCA programme/Generalitat de Catalunya. The ICN2 is supported by the Severo Ochoa Centres of Excellence programme, Grant CEX2021-001214-S, funded by MCIN/AEI/10.13039.501100011033. E. Calucho acknowledges Ministerio de Ciencia e Innovación of Spain and Fondo Social Europeo for the Fellowship PRE2018-084856 awarded under the call "Ayudas para contratos predoctorales para la formación de doctors, Subprograma Estatal de Formación del Programa Estatal de Promoción del Talento y su Empleabilidad en I + D + i", under the framework of "Plan Estatal de Investigación Científica y Técnica y de Innovación 2017–2020". E. Calucho also acknowledges Universitat Autònoma de Barcelona (UAB) for the possibility of performing this work inside the framework of Biotechnology PhD Programme. M. Rossetti is supported from the European Union's Horizon 2020 research and innovation programme under the Marie Skłodowska-Curie grant agreement No 101029884 (SERENA). We acknowledge Departament de Recerca i Universitats of Generalitat de Catalunya for the grant 2021 SGR 01464 and Grant PID2021-124795NB-I00 funded by MCIN/AEI/10.13039/501100011033 and by "ERDF A way of making Europe".

The authors would like to acknowledge Dr. Belén Ballesteros and Marcos Rosado for their support and assessment on obtaining EDX and SEM images, respectively. Antti Tullila (currently Aidian Oy) and Kristiina Iljin (VTT) are thanked for preparing the cortisol-albumin conjugate and purification of the anti-cortisol (17) Fab, respectively.

Appendix A. Supplementary data

Supplementary data to this article can be found online at https://doi.org/10.1016/j.bios.2024.116315.

References

Arlt, W., Allolio, B., 2003. Lancet 361, 1881–1893.

Baptista-Pires, L., Mayorga-Martínez, C.C., Medina-Sánchez, M., Montón, H., Merkoçi, A., 2016. ACS Nano 10, 853–860.

Budd, J., Miller, B.S., Weckman, N.E., Cherkaoui, D., Huang, D., Decruz, A.T., Fongwen, N., Han, G.-R., Broto, M., Estcourt, C.S., Gibbs, J., Pillay, D., Sonnenberg, P., Meurant, R., Thomas, M.R., Keegan, N., Stevens, M.M., Nastouli, E., Topol, E.J., Johnson, A.M., Shahmanesh, M., Ozcan, A., Collins, J.J., Fernandez Suarez, M., Rodriguez, B., Peeling, R.W., McKendry, R.A., 2023. Nat. Rev. Bioeng. 1, 13–31.

Calucho, E., Parolo, C., Rivas, L., Álvarez-Diduk, R., Merkoçi, A., 2020. Compr. Anal. Chem. 313–359.

Cheng, J., Yang, G., Guo, Jiuchuan, Liu, S., Guo, Jinhong, 2022. Analyst 147, 554–570.

de Freitas, I.C., Parreira, L.S., Barbosa, E.C.M., Novaes, B.A., Mou, T., Alves, T.V., Quiroz, J., Wang, Y.-C., Slater, T.J., Thomas, A., Wang, B., Haigh, S.J., Camargo, P. H.C., 2020. Nanoscale 12, 12281–12291.

De La Escosura-Muñiz, A., Parolo, C., Maran, F., Merkoçi, A., 2011. Nanoscale 3, 3350–3356.

Deenin, W., Yakoh, A., Pimpitak, U., Pasomsub, E., Rengpipat, S., Crespo, G.A., Chaiyo, S., 2023. Bioelectrochemistry 152, 108438.

Du, D., Wang, J., Wang, L., Lu, D., Lin, Y., 2012. Anal. Chem. 84, 1380–1385.

El-Kady, M.F., Strong, V., Dubin, S., Kaner, R.B., 2012. Science 335, 1326–1330.

Elgrishi, N., Rountree, K.J., McCarthy, B.D., Rountree, E.S., Eisenhart, T.T., Dempsey, J. L., 2018. J. Chem. Educ. 95, 197–206.

Eronen, V., Tullila, A., Iljin, K., Rouvinen, J., Nevanen, T.K., Hakulinen, N., 2023. J. Struct. Biol. 215, 107966.

Fu, W., Jiang, L., van Geest, E.P., Lima, L.M.C., Schneider, G.F., 2017. Adv. Mater. 29, 1–25.

Giacomelli, C., Álvarez-Diduk, R., Testolin, A., Merkoçi, A., 2020. 2D Mater. 7, 024006.

Gonzalez-Macia, L., Li, Y., Zhang, K., Nunez-Bajo, E., Barandun, G., Cotur, Y., Asfour, T., Olenik, S., Coatsworth, P., Herrington, J., Güder, F., 2023. bioRxiv 2023.03.09.531916.

Hellhammer, D.H., Wüst, S., Kudielka, B.M., 2009. Psychoneuroendocrinology 34, 163–171.

Jang, H.J., Sui, X., Zhuang, W., Huang, X., Chen, M., Cai, X., Wang, Y., Ryu, B., Pu, H., Ankenbruck, N., Beavis, K., Huang, J., Chen, J., 2022. ACS Appl. Mater. Interfaces 14, 24187–24196.

Jang, H.J., Zhuang, W., Sui, X., Ryu, B., Huang, X., Chen, M., Cai, X., Pu, H., Beavis, K., Huang, J., Chen, J., 2023. ACS Appl. Mater. Interfaces 15, 15195–15202.

Kudr, J., Zhao, L., Nguyen, E.P., Arola, H., Nevanen, T.K., Adam, V., Zitka, O., Merkoçi, A., 2020. Biosens. Bioelectron. 156, 112109.

Muhammad-Tahir, Z., Alocilja, E.C., 2003. Biosens. Bioelectron. 18, 813–819.

Nandhakumar, P., Muñoz San Martín, C., Arévalo, B., Ding, S., Lunker, M., Vargas, E., Djassemi, O., Campuzano, S., Wang, J., 2023. ACS Sensors.

Oelkers, W., 1996. N. Engl. J. Med. 335, 1206–1212.

Parolo, C., Merkoçi, A., 2013. Chem. Soc. Rev. 42, 450–457.

Parolo, C., Sena-Torralba, A., Bergua, J.F., Calucho, E., Fuentes-Chust, C., Hu, L., Rivas, L., Álvarez-Diduk, R., Nguyen, E.P., Cinti, S., Quesada-González, D., Merkoçi, A., 2020. Nat. Protoc. 15, 3788–3816.

Perju, A., Wongkaew, N., 2021. Anal. Bioanal. Chem. 413, 5535–5549.

Preechakasedkit, P., Panphut, W., Lomae, A., Wonsawat, W., Citterio, D., Ruecha, N., 2023. Anal. Chem. 95, 13904–13912.

Reiner-Rozman, C., Kotlowski, C., Knoll, W., 2016. Biosensors 6, 1–12.

Ricci, F., Adornetto, G., Palleschi, G., 2012. Electrochim. Acta 84, 74–83.

Rivas, L., de la Escosura-Muñiz, A., Pons, J., Merkoçi, A., 2014. Electroanalysis 26, 1287–1294.

Rivas, L., Hu, L., Parolo, C., Idili, A., Merkoçi, A., 2023. ACS Appl. Nano Mater. 6, 4151–4161.

Ruiz-Vega, G., Kitsara, M., Pellitero, M.A., Baldrich, E., del Campo, F.J., 2017. Chemelectrochem 4, 880–889.

Sakihara, S., Kageyama, K., Oki, Y., Doi, M., Iwasaki, Y., Takayasu, S., Moriyama, T., Terui, K., Nigawara, T., Hirata, Y., Hashimoto, K., Suda, T., 2010. Endocr. J. 57, 331–337.

Scroccarello, A., Álvarez-Diduk, R., Della Pelle, F., de Carvalho Castro e Silva, C., Idili, A., Parolo, C., Compagnone, D., Merkoçi, A., 2023. ACS Sens. 8, 598–609.

Sena-Torralba, A., Álvarez-Diduk, R., Parolo, C., Piper, A., Merkoçi, A., 2022. Chem. Rev. 122, 14881–14910.

Soni, M., Kumar, P., Pandey, J., Sharma, S.K., Soni, A., 2018. Carbon N. Y. 128, 172–178.

Tanimoto, S., Ichimura, A., 2013. J. Chem. Educ. 90, 778–781.

Weiß, L.J.K., Lubins, G., Music, E., Rinklin, P., Banzet, M., Peng, H., Terkan, K., Mayer, D., Wolfrum, B., 2022a. ACS Sens. 7, 884–892.

Weiß, L.J.K., Rinklin, P., Thakur, B., Music, E., Url, H., Kopic, I., Hoven, D., Banzet, M., Von Trotha, T., Mayer, D., Wolfrum, B., 2022b. ACS Sens. 7, 1967–1976.

Zhao, C., Fan, L., 2012. Microchim. Acta 178, 107–114.

Zhao, L., Rosati, G., Piper, A., de Carvalho Castro e Silva, C., Hu, L., Yang, Q., Della Pelle, F., Alvarez-Diduk, R.R., Merkoçi, A., 2023. ACS Appl. Mater. Interfaces 15, 9024–9033.